

Detecting extra-galactic supernova neutrinos in the Antarctic ice

Sebastian Böser*, Marek Kowalski, Lukas Schulte, Nora Linn Strotjohann, Markus Voge

Physikalisches Institut, Universität Bonn, D-53115 Bonn, Germany

Abstract

Building on the technological success of the IceCube neutrino telescope, we outline a prospective low-energy extension that utilizes the clear ice of the South Pole. Aiming at a 10 Mton effective volume and a 10 MeV threshold, the detector would provide sufficient sensitivity to detect neutrino bursts from core-collapse supernovae (SNe) in nearby galaxies. The detector geometry and required density of instrumentation are discussed along with the requirements to control the various sources of background, such as solar neutrinos. In particular, the suppression of spallation events induced by atmospheric muons poses a challenge that will need to be addressed. Assuming this background can be controlled, we find that the resulting detector will be able to detect SNe from beyond 10 Mpc, delivering between 10 and 41 regular core-collapse SN detections per decade. It would further allow to study more speculative phenomena, such as optically dark (failed) SNe, where the collapse proceeds directly to a black hole, at a detection rate similar to that of regular SNe. We find that the biggest technological challenge lies in the required number of large area photo-sensors, with simultaneous strict limits on the allowed noise rates. If both can be realized, the detector concept we present will reach the required sensitivity with a comparatively small construction effort and hence offers a route to future routine observations of SNe with neutrinos.

Keywords: supernovae, core-collapse, neutrino physics, neutrino detectors

1. Introduction

In 1987, Supernova 1987A (SN 1987A) exploded in the Large Magellanic Cloud at a distance of only 50 kpc, leading to the first detection of neutrinos from outside our solar system. Despite the fact that only ~ 20 supernova neutrinos were detected in total [1], a wealth of papers has been published in its wake (see e.g. [2] for a summary), reflecting the numerous and fundamental roles that neutrinos play in astrophysics as well as in particle physics (e.g. see [3, 4]).

Given today's detectors, a supernova in our Galaxy would result in $\sim 10^4$ neutrino events detected individually in Super-Kamiokande [5] and other large low-energy neutrino detectors, as well as up to millions of neutrinos detected through an increase in noise rate in IceCube [6]. However, with an expected rate of only 1-3 Galactic SNe per century [7, 8], the chance for a detection during the lifetime of the experiments is not overwhelmingly large. In the fortunate case of a SN detection, the uniqueness of the progenitor system will make it difficult to disentangle the astrophysical diversity from the effects due to particle physics (e.g. neutrino oscillations) that will impact the light curve and energy spectra.

As pointed out in [7] and [8], the situation will change drastically once neutrino detectors reach the sensitivity

threshold to detect “mini-bursts” of neutrinos from supernovae in neighboring galaxies. Not bound to our own Galaxy, the rate of SN observations will depend only on the size of the detectors. As we will show in Section 6, an effective volume of ~ 10 Mtons is sufficient to detect SNe at a rate of $\sim 1 - 4$ per year—albeit most of them with less than ten individual neutrino events. Despite the low number of detected neutrinos, these routine observations would provide a wealth of information and allow entirely new studies [8]. What follows is a brief and incomplete summary of the scientific benefits of a large supernova neutrino detector.

The total SN rate in our local universe would be determined in a novel and less biased way. Given an apparent mismatch in rates—only about half the expected rate of SNe is actually detected by optical surveys [9]—a direct measurement would solve the riddle of missing supernovae.

Furthermore, a sufficiently sensitive detector allows us to test models predicting additional neutrino bursts, such as failed or *dark* (i.e. optically unobservable) SNe [10], merger of binary neutron stars [11] or the formation of quark stars [12]. Dark SNe are core-collapse objects that directly form a black hole (BH). Electromagnetic radiation is strongly suppressed, since the photons don't have time to escape and are swallowed by the forming BH. Neutrinos, on the other hand, can escape, and the expected burst from such an event is both more luminous and hotter [10]. Average neutrino energies can be roughly twice as large as in the case of the collapse to a neutron star (NS)

*Email: sboeser@physik.uni-bonn.de

and hence open the opportunity to identify the collapse to a BH. Another opportunity is the identification of questionable optical SN candidates, e.g. luminous blue variables [13], as “supernova impostors” by the non-detection of neutrinos [8].

In addition, detections of neutrino bursts can be used to trigger early optical or X-ray observations. Having a precise timing for the moment of explosion and observing the shock-breakout in electromagnetic radiation, will allow to infer a wealth of information about the progenitor system. In the absence of a direction for the SN, the follow-up could focus on observation of nearest galaxies, since these are the only ones for which a neutrino detection is expected.

With a larger number of supernova neutrinos, even a broader physics program can be accessed. Due to the complexity of the involved processes, modeling of supernova explosions is still a challenge today and has significant variance in e.g. the predicted mean neutrino energy [14]. Determination of the neutrino luminosity and energy spectrum will provide valuable input to these models.

From the observation of the arrival times of the neutrinos from SN 1987A, a limit in the eV range has been set on the effective mass of the anti-electron neutrino [15]. By observing neutrinos from supernovae with higher statistics, more stringent limits could be set. In addition, by its impact on the predicted flux, the neutrino mass hierarchy can be addressed as well, provided a sufficient number of neutrinos is observed [6].

Motivated by this scientific potential, several megaton scale neutrino detectors are currently planned (e.g. DeepTITAND [8], Hyper-Kamiokande [16, 17] and UNO [18]). Those are either water Cherenkov detectors located in mines or marine detectors, similar to ANTARES [19]. In this paper, we explore the potential of a ~ 10 Mton detector in the Antarctic ice shield. In the existing IceCube detector that has been optimized for TeV-PeV energies [20], SN neutrino bursts are typically searched for by looking for a collective enhancement of photomultiplier noise rates [6]. Due to the large sensor spacing and consequently high energy threshold, attempting to detect individual neutrino events in this configuration significantly reduces the effective mass and hence distance at which SNe can be detected [21]. A dedicated effort is now under way to reduce the energy threshold to a few GeV in the PINGU (Phased IceCube Next-Generation Upgrade) project [22], with one of its goals being the determination of the neutrino mass hierarchy through the MSW effect [23]. Building on this effort and the expertise accumulated with IceCube and AMANDA [24–27], we explore the capabilities of a dedicated low-energy extension to study individual supernova neutrino events. The challenge is to reduce the energy threshold of the experiment by three orders of magnitude while controlling the background at a level required for the detection of supernovae.

While we will focus on this aspect in this paper, it

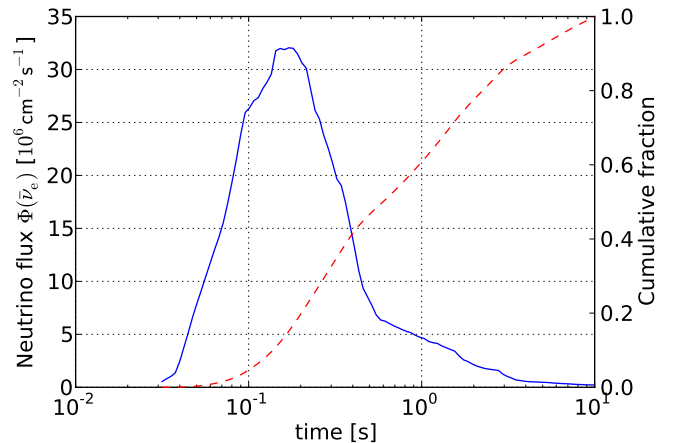


Figure 1: Time evolution of $\bar{\nu}_e$ flux for a SN at 1 Mpc in the Lawrence-Livermore model [30] (full line represents the differential flux and dashed line the integral).

should be noted that such a detector will not be limited to the detection of neutrinos at a few MeV, but will also provide unprecedented sensitivity at the GeV-scale. Not only the neutrino oscillation sector will be accessible with increased precision — it will also provide sensitivity to other astrophysical phenomena such as collisional heating in gamma-ray bursts [28, 29].

The paper is organized as follows: The SN models that we use to benchmark a future detector are discussed in Section 2, followed by a description of our detector simulation and the optimization of the detector configuration in Section 3. Section 4 is a discussion of the various background sources that can be anticipated while Section 5 investigates an alternative detector depth. Finally, we give an estimate on the expected SN rate in Section 6 and conclude with a discussion of the results in Section 7.

2. Neutrinos from core-collapse supernovae

In core-collapse supernovae, neutrinos are produced in course of the formation of a neutron star which follows the gravitational collapse of a massive progenitor star. Electrons and protons rapidly fuse to neutrons, emitting electron neutrinos, which results in a sharp (~ 10 ms) depletion peak in the neutrino flux which marks the birth of the neutron star. However, most supernova neutrinos ($\sim 90\%$) originate from thermal pair creation [31]. These neutrinos, released over a characteristic diffusion time of 1-10 s (cf. Fig. 1), are of all flavors, with flavor ratios, light curve and energy spectrum still being under debate [14].

An early simulation of neutrino production in SN explosions has been provided in the so-called Lawrence Livermore (LL) model [30]. In the LL model, the neutrino

	Mass [M_{\odot}]	$\langle E_{\bar{\nu}_e} \rangle$ [MeV]	$\beta_{\bar{\nu}_e}$	$L_{\bar{\nu}_e}$ [erg]
LL SN	20	15.4	3.8	$4.9 \cdot 10^{52}$
TBP SN	11 and 15	11.4	3.7	$(4.9 \cdot 10^{52})$
Dark SN	25 – 40	20 – 24	-	$\sim 10^{53}$

Table 1: Parameters of the Lawrence Livermore (LL) model [2], the Thompson, Burrows, Pinto (TBP) model [32] and the dark supernova model [10] for the neutrino spectrum of a core-collapse supernova. The table presents the stellar mass of the progenitor M_{\odot} , the average neutrino energy $\langle E_{\bar{\nu}_e} \rangle$, the pinch parameter $\beta_{\bar{\nu}_e}$ (see Eqn. 1) and the time-integrated luminosity in anti-electron neutrinos $L_{\bar{\nu}_e}$. The TBP model does not lead to an explosion, i.e. no luminosity emerges from the simulation. Instead, the luminosity from the LL model is assumed. Please note that for dark SNe Eqn. 1 is not valid, instead the positron spectrum given in [10] was used.

spectrum is parametrized by

$$\frac{dN}{dE} = \frac{(1 + \beta)^{1 + \beta} L}{\Gamma(1 + \beta) \langle E \rangle^2} \left(\frac{E}{\langle E \rangle} \right)^{\beta} \exp \left(-(1 + \beta) \frac{E}{\langle E \rangle} \right), \quad (1)$$

where L is the luminosity and $\langle E \rangle$ the average energy while β determines the width of the spectrum. The parameters for the LL simulation as well as for a competing model by Thompson, Burrows and Pinto (TBP) [32] are reproduced in Table 1. While the latter model does not result in an explosion of the supernova, [14] suggests that the resulting luminosity should be of the same order of magnitude. A large variety of other neutrino emission models exists [33], but we restrict ourselves to these two commonly used ones for ease of comparison. Alternative models predicting low-energy neutrinos include *dark supernovae* in which stars heavier than $\sim 25 M_{\odot}$ form black holes. It is assumed that if the progenitor does not rotate fast enough to explode as a hypernova, it will be very faint or even dark in optical emission, while even more luminous in neutrino flux than ordinary supernovae [34, 35]. The resulting neutrinos have average energies of $\langle E_{\nu} \rangle \sim 20 - 24$ MeV [10].

The neutrinos from the different collapse scenarios can best be detected via inverse beta decay (IBD)



that requires a threshold energy of $E_{\nu} > 1.806$ MeV. We use the approximation for the energy dependence of the cross-section called “Naïve +”, which is presented in [36]. Since the cross-section rises with energy, the resulting positron spectrum is harder than the initial neutrino spectrum. Figure 2 shows the resulting positron spectra for the two different supernova models as well as for a model of dark supernovae. Neutrino oscillations, which harden the spectrum, are taken into account only for the dark model, for which we directly take the positron spectrum from [10].

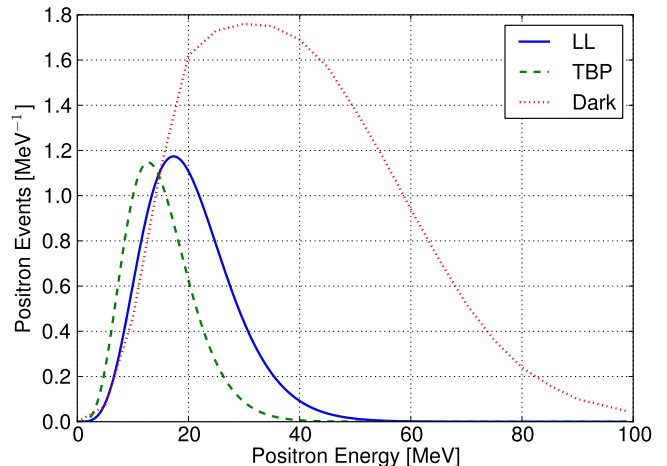


Figure 2: Positron spectrum for the Lawrence-Livermore (LL) [30], Thompson, Burrows, Pinto (TBP) [32] and a dark supernova model [10] for a SN at 1 Mpc and an effective detector volume of 1 Mton.

For a typical positron energy of 20 MeV, the corresponding track length is ~ 10 cm in ice, resulting in ~ 3600 Cherenkov photons (300–600 nm) [6]. Since the light yield scales linearly with the positron track length, and hence with the positron energy, the average amount of light produced per neutrino is model dependent.

3. Detector simulation and optimization

In this section we describe the simulation and optimization of a possible optical Cherenkov detector array in the Antarctic ice, capable of detecting MeV neutrinos with high statistics. The geometry of the detector as sketched in Figure 3 consists of 127 vertical strings, arranged in a filled hexagon, similar to IceCube and corresponding to a construction period of ~ 5 years. Fuel costs dominate the drilling expenses which amount to about 0.5M\$ per hole. While the number of strings is comparable, closer horizontal spacing of the strings than in IceCube is required. We optimize this spacing between 10 and 40 m for the best effective detection volume. For the vertical position of the optical sensors we choose the ice layer between 2150 and 2450 m below the surface, where also the DeepCore array is located. At this depth, air bubbles have fully degenerated due to the high ambient pressure and only a small dust concentration was measured [37, 38]. Consequently, the ice in these depths has the largest scattering lengths of $\lambda_e \approx 20 - 50$ m. The absorption length is $\lambda_a \approx 20 - 90$ m, depending on wavelength [37, 38].

These excellent optical properties—comparable to what can be achieved in laboratory conditions—allow for an efficient photon detection as well as precise reconstruction of the event position and direction. For an accurate simulation of the photon propagation in this environment, we use

the *Photonics code* [39–41]—a parametric simulation developed for IceCube. It includes the full depth-dependence of the scattering and absorption properties of the ice [37].

IceCube employs photo-sensors, so-called digital optical modules (DOMs) [42], each including a 10" Hamamatsu PMT integrated into a pressure-resistant glass sphere that also includes the electronics for HV generation and in-ice digitalization of the PMT signal. The dark noise rate of individual DOMs averages around 500 Hz [6]. IceCube DOMs have a non-trivial directional sensitivity [43] which is incorporated in the Photonics simulation package [41] and hence included in our simulation. Both regular efficiency and high quantum efficiency (HQE) PMTs are deployed in IceCube. From laboratory measurements [44], we obtain an effective area¹ of 19.4 (26.3) cm² for an IceCube DOM equipped with a regular (HQE) PMT.

Due to the comparatively low energy of supernova neutrinos and the corresponding small light yield, a high density of photo-sensitive area is required to obtain acceptable trigger rates. We find that even for the closest possible vertical spacing of one HQE optical module per meter on our 300 m long strings and the closest possible horizontal string spacing of 10 m, the effective mass for neutrino detection falls short of our 10 Mton target (c.f. Fig. 6). Instead, we simulate photodetectors with an effective area equivalent to ≈ 5.4 HQE IceCube optical modules per meter. While the use of significantly larger photocathode area may be challenging and is in particular limited by the achievable drill hole diameter, on-going R&D for larger effective area and cheaper optical modules with less noise based on wavelength shifters shows promising first results[45].

Neutrinos are simulated employing a Monte Carlo method where interaction vertices are generated homogeneously within and beyond the detector volume. The positron energy is sampled according to one of the energy spectra shown in Fig. 2. Using the Photonics code, we first calculate the average number of detected photons for each sensor, given the neutrino vertex and positron energy. The actual number of detected photons is then drawn from a Poisson distribution and the hit times are sampled for each of these photons from the respective arrival time distribution.

In order to optimize the detector geometry, the effective positron detection mass is calculated as function of the lateral spacing between strings. The *effective mass* is the mass of the geometrical simulation volume multiplied with the fraction of simulated events that are detected above threshold. This threshold is set at a minimum of five photo-sensors being hit by photons, and was chosen to allow for reconstruction of the vertex position and positron direction which correspond to five degrees of freedom. Generally, one finds that, as the string distance increases, the geometrical detector volume increases, but the fraction

¹Averaged over all incident angles and wavelengths, assuming isotropic emission with a Cherenkov spectrum $\propto \lambda^{-2}$.

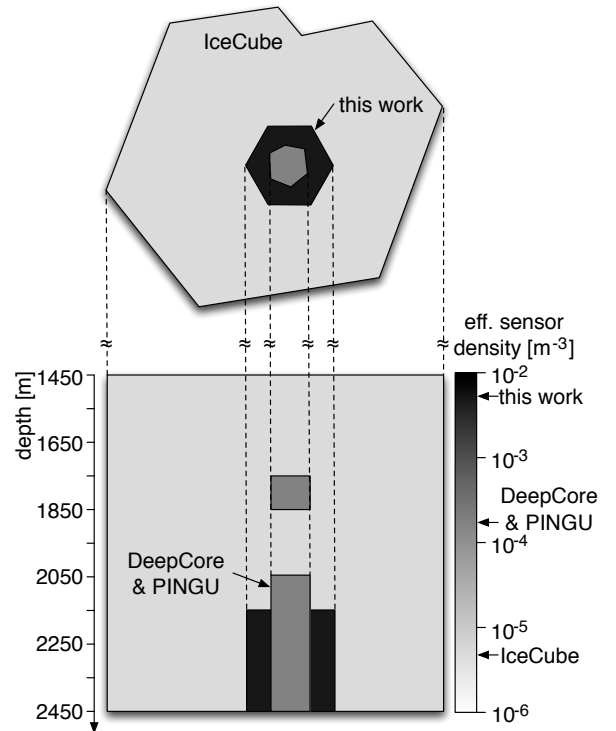


Figure 3: Dimensions and effective sensor density of the aspired detector with 127 strings and 25 m string spacing as compared to IceCube and PINGU/DeepCore. The gray-scale effective sensor density indicates the installed photo-effective area per m³ in units of HQE IceCube DOMs.

of detected neutrino events with at least five hit sensors decreases, yielding a maximum effective volume of ~ 18 Mton for a string spacing around 30 m for a Lawrence-Livermore neutrino spectrum.

4. Background studies

Up to this point, we have solely implied the trigger requirement—that the number of sensors hit by photons be at least five for each neutrino event. In this section, we will discuss the dominant sources of background and how they can be controlled by implying additional constraints on the distribution of photon hits. Contributions from random noise, atmospheric neutrinos, atmospheric muons, and solar neutrinos are considered.

Neutrinos from SNe come in bursts. To be distinguished from uncorrelated background or noise triggers, a SN will need to produce a certain multiplicity of neutrino triggers within a given time window. We can claim a supernova detection if a certain number of trigger events N_ν occur within a time window of $\Delta t_{SN} \sim 1-10$ s (c.f. Figure 1). Under the constraint that we want a limited amount of false SN detections, N_ν and Δt_{SN} determine the maximally allowed background/noise trigger rate f_{noise} . The

N_ν	Δt_{SN} [s]	f_{noise} [mHz]
3	10	0.86
4	10	3.74
5	10	9.61

Table 2: Maximally allowed noise/background trigger rate f_{noise} for an average of 1 false SN event per year, consisting of N_ν events falling into a time window of Δt_{SN} .

number of false SN detections per year N_{SN} as function of f_{noise} , N_ν and Δt_{SN} is:

$$N_{\text{SN}} = f_{\text{noise}} \cdot (1 - P_{\text{cdf}}(N_\nu - 2, \mu = f_{\text{noise}} \Delta t_{SN})) \cdot 1 \text{ yr} \quad (3)$$

where P_{cdf} is the cumulative Poisson distribution. If we want to limit the false SN detection rate to about 1 per year, comparable to the expected signal SN detection rate, we get the maximally allowed noise rates shown in Table 2. E.g., we can accept at most ≈ 0.9 mHz of background/noise trigger rate if we want to detect a SN with 3 neutrino events within 10 s. In the following estimates, we will use the rounded value of 1 mHz as the tolerable upper limit on the noise and background rates.

4.1. Sensor noise

Since the Antarctic ice shield is a very low-radioactivity environment, the main sources of random noise are introduced by the detector itself: radioactive isotopes and thermal noise in the photo-sensors and electronics. For the IceCube modules, this results in a dark count rate of ~ 500 Hz [6]. It is known that some fraction of the noise is not purely random, but correlated in time, however we will neglect this for the sake of simplicity.

As mentioned above, the detector presented here will not be feasible using IceCube modules. New photo-sensor technologies (e.g. based on wavelength shifters as light collectors) are currently discussed for deployment in future extensions to IceCube [45], that offer increased effective photo-sensitive area in combination with a significantly reduced noise rate. These technologies are still in the design phase, so the achievable noise rate is not known yet. We use dark noise values of 500 Hz, 50 Hz and 10 Hz as templates in absence of solid numbers.

As shown in Table 2, the rate f_{noise} of background neutrino triggers caused by random noise hits has to be below ≈ 1 mHz if only one false 3-neutrino supernova burst detection is tolerated per year. We calculate this noise trigger rate depending on the total number of modules in the detector N_{tot} , the random noise rate per module f_m , the number of hit modules n_{trig} that is required for a neutrino event to trigger and the trigger time window t_{trig} . Assuming that one module has registered a random noise hit and opened the trigger window, the probability P_m for any module to also see at least one noise hit during this

time window t_{trig} is complementary to the probability to register no hit, which will follow a Poisson distribution:

$$P_m = 1 - e^{-f_m \cdot t_{\text{trig}}}. \quad (4)$$

The probability for a noise event P_{noise} is the probability that at least $n_{\text{trig}} - 1$ more modules also encounter a noise hit in the time window. Using the binomial distribution, again via the complementary probability of registering $n_{\text{trig}} - 2$ noise hits or less:

$$P_{\text{noise}} = 1 - B_{\text{cum}}(n_{\text{trig}} - 2 | N_{\text{tot}}, P_m), \quad (5)$$

where $B_{\text{cum}}(m | n, p) = \sum_{k=0}^m \binom{n}{k} p^k (1-p)^{n-k}$ is the cumulative binomial probability for up to m successes out of n tries with probability p . Apart from boundary effects, the rate of noise triggers in the detector is then

$$f_{\text{noise}} = P_{\text{noise}} \cdot f_m \cdot N_{\text{tot}}. \quad (6)$$

Using generic values for the dark count $f_m = 500$ Hz, $N_{\text{tot}} = 38100$ for a detector with 127 strings and 300 modules per string, and requiring $n_{\text{trig}} = 5$ hits in $t_{\text{trig}} = 1000$ ns, the rate of false SN events is $f_{\text{noise}} = 19$ MHz, i.e. 10 orders of magnitude above the allowed value from Table 2. Even assuming a module dark noise rate as low as $f_m = 10$ Hz, still $f_{\text{noise}} = 247$ Hz, well in excess of what can be tolerated. This clearly shows that it is necessary to apply intelligent trigger algorithms that take advantage of the non-uniform distribution of photons from neutrino interaction and thus limit the number of modules considered by the trigger. In the following, we present two strategies that reject events induced by sensor noise.

4.1.1. Local coincidence cleaning (RT)

Noise hits are uniformly distributed across the detector while signal hits follow a certain topology: A positron from inverse beta decay produces Cherenkov light along its few cm long track. We can consider the positrons to be point sources of light that is scattered in the ice. These events are thus characterized by hits spreading roughly spherically from the vertex, with a preferred direction due to the Cherenkov cone.

We can exploit this topology of the signal hits. As demonstrated for IceCube, requiring a local coincidence between photon hits is a very efficient way to reduce the effect of random noise [46]. A hit is required to be accompanied by at least another hit within a certain radius r_{RT} and time window t_{RT} in order to fulfill the local coincidence criterion. Fig. 4 shows an illustration of this radius-time (RT) requirement. The hit cleaning was found to indeed reduce the noise trigger rate while keeping most of the signal events. The parameters t_{RT} and r_{RT} are optimized for the maximum effective mass at each string spacing d_{str} .

4.1.2. Phase space cut (PS)

The local coincidence cleaning selects hits that are likely causally connected, i.e. close to each other in time and

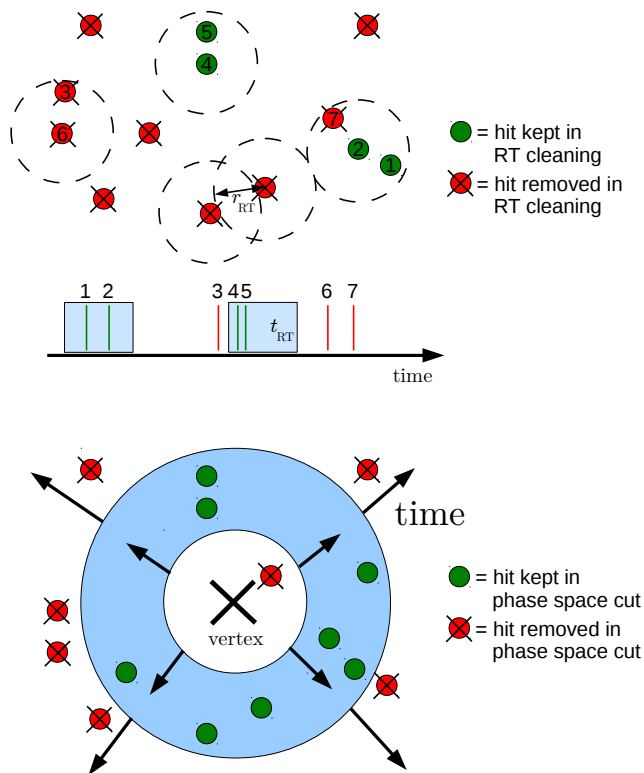


Figure 4: Illustration of the local coincidence (RT) cleaning and the phase space (PS) cut. Each colored sphere corresponds to a hit optical module. Dashed circles indicate the radius r_{RT} , blue boxes the time window t_{RT} of the local coincidence cleaning. The blue region marks the expanding spherical shell used in the phase space cut.

space. However, this does not take into account the global signal hit distribution in the detector. As photons propagate away from the vertex, the photon distribution can be roughly modeled as an expanding spherical shell. The rate of noise events can be significantly reduced by defining a fiducial detector volume (the spherical shell) and accepting only hits within this volume for the trigger.

This fiducial volume is defined relative to the time and position of the neutrino vertex. Since the vertex is not known a priori, we use a χ^2 -minimization of the residual time, i.e. the photon propagation time minus the expected photon propagation time for straight travel from the vertex, to reconstruct the vertex position. Using this simple method, a positional resolution of ~ 15 m can be achieved. To incorporate this limited knowledge of the vertex position, a random Gaussian smearing with 10 m standard deviation in each coordinate is applied to the vertex position of our simulated events. Fig. 5 shows the distribution of hits in the two-dimensional phase space (PS) given by the time between the hit and the neutrino interaction and

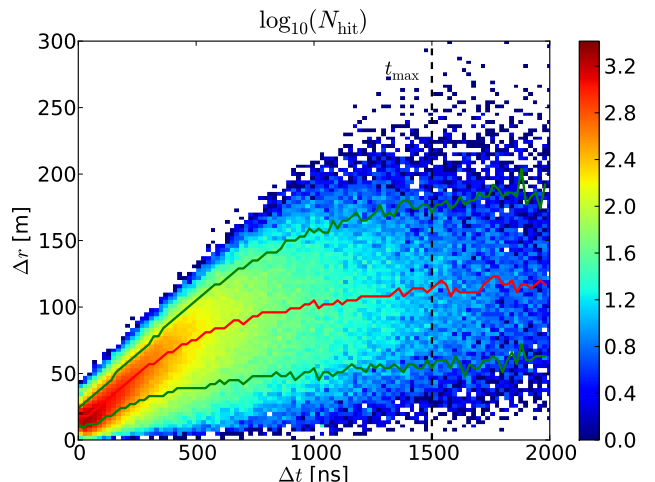


Figure 5: Distribution of signal hits in the simulated detector: spatial distance Δr to the vertex position vs. time difference Δt between the hit and the neutrino interaction.

the distance between the hit module and the reconstructed vertex. The 10% and 90% quantiles of the distance are calculated for each time (green lines in Fig. 5, red line is the median) and give the inner and outer radius of our fiducial volume (cf. Fig. 4). The resulting spherical shell expands with time and contains $\approx 80\%$ of the signal hits. Since all photons are eventually absorbed, we cut the fiducial volume at time t_{max} .

As the phase space volume (i.e. the number of sensors contributing to the trigger) quickly increases with t_{max} , the noise trigger rate f_{noise} rapidly rises with t_{max} as well. We choose the value of t_{max} so that it limits $f_{noise} \leq 1$ mHz for a given sensor noise rate f_m .

Under this constraint, we simultaneously optimize the number of hits required to form a trigger n_{trig} , the string spacing d_{str} of the detector, the cleaning radius and time (r_{RT} and t_{RT}), and t_{max} in order to maximize the effective mass for SN signal neutrinos.

4.1.3. Conclusion

Fig. 6 shows the resulting effective mass after the two self-noise cuts have been applied, Tab. 3 lists the optimal parameters as function of module noise f_m . While this method reduces the trigger efficiency for neutrino interaction by up to a factor of about 4, at the same time the noise trigger rate is reduced by many orders of magnitude. For the module dark noise rate of 500 Hz, as provided by IceCube DOMs, the effective mass of this detector configuration falls short of the initial target of 10 Mton. In order to retain 10 Mton, reducing the sensor self-noise rate to $\lesssim 50$ Hz per meter instrumented string (350 mHz/cm² effective photo-sensitive area) is desirable.

While more advanced algorithms considering the full event topology would still allow for a moderate increase

of the effective mass, this study demonstrates the importance of both large photo-sensitive area and at the same time low noise optical sensors, posing quite a technological challenge. Correlated noise that was not treated here will be more difficult to reject and provides additional motivation to seek low dark noise rates in future photo-sensor R&D. In the following, we assume a module noise rate of 10 Hz.

4.2. Muon background

Muons crossing the detector or passing nearby are easily separable from the SN neutrino signal via the huge amount of Cherenkov light produced by the extended track. An additional outer layer of photosensitive modules, naturally provided by IceCube, will ensure that even muons passing by at large distances or stopping just above the detector can be identified as such and be vetoed.

For a conservative first estimate of the dead time caused by atmospheric muons, we assume all muons reaching the top of the detector being energetic enough to cross it. From [47] we obtain a muon flux of $\Phi_\mu = 8 \cdot 10^{-8} \text{ cm}^{-2} \text{ s}^{-1} \text{ sr}^{-1}$ for the top of the detector at 2150 m depth, giving a muon passing rate of about

$$R_\mu = \Phi_\mu \cdot 300 \text{ m} \times 300 \text{ m} \cdot \pi \approx 230 \text{ Hz} \quad (7)$$

using a detector cross-sectional area of $(300 \text{ m})^2$ and an effective solid angle of π that accounts for the lower flux from angles closer to horizon where the ice shield is thicker. A muon traveling through the entire detector has a track length of $\approx 300 \text{ m}$ and emits about $N_0 \approx 10^7$ Cherenkov photons on its path (≈ 360 photons per cm). We assume as a worst case that all photons are trapped within the detector volume by scattering to compute how long the photons will remain detectable within the detector before

	f_m	[Hz]	10	50	500
optimized parameters	d_{str}	[m]	25	25	25
	n_{trig}		5	5	5
	r_{RT}	[m]	115	85	40
	t_{RT}	[ns]	1200	400	250
	t_{max}	[ns]	1590	850	390
properties	f_{noise}	[Hz]	1.0	3.4	$2.2 \cdot 10^4$
	$f_{\text{noise}}^{\text{cut}}$	[mHz]	1	1	1
	M_{eff}	[Mton]	13.1	10.5	5.4

Table 3: Optimal parameters for string spacing (d_{str}), required hit multiplicity (n_{trig}), RT cleaning radius (r_{RT}) and time (t_{RT}) as well as maximum hit time window (t_{max}) together with resulting effective mass M_{eff} as function of module noise rate f_m . The parameters are chosen such that RT cleaning and phase space cut limit the rate of noise triggers f_{noise} down to $f_{\text{noise}}^{\text{cut}} = 1 \text{ mHz}$.

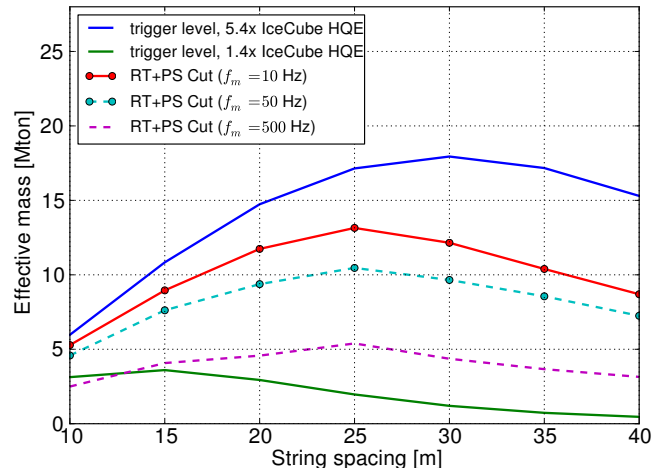


Figure 6: Effective mass at trigger level with modules having 1.4 (lower solid) and 5.4 times the effective area of IceCube HQE DOMs (upper solid). The same after applying radius-time (RT) cleaning and phase space (PS) cut for different module noise rates (solid with bullets, dashed). The noise cleaning is done such that a noise trigger rate of about 1 mHz remains, a dead time of 0.16% due to atmospheric muons is included.

they are absorbed. The number of photons after a path $x = ct/n$ is given by:

$$N_\gamma = N_0 \cdot e^{-\frac{x}{\lambda_a}}, \quad (8)$$

with $t_{\text{abs}} = n \lambda_a / c = 0.44 \cdot 10^{-6} \text{ s}$, for an absorption length of $\lambda_a \lesssim 100 \text{ m}$ and a refractive index of $n = 1.31$. After a time

$$t = t_{\text{abs}} \ln \frac{N_0}{N_\gamma} \approx 7 \mu\text{s} \quad (9)$$

the number of unabsorbed photons in the detector due to a crossing muon has fallen below $N_\gamma = 1$ which is well below our trigger threshold. We therefore conservatively assume each passing muon to illuminate the detector for a time interval of $7 \mu\text{s}$ which can be considered as dead time for supernova neutrino detection, corresponding to a fraction of $R_\mu \cdot 7 \mu\text{s} = 0.16\%$ of detector operation time.

Passing muons are easily identified because of the dense instrumentation and can be rejected applying a veto. However, muons also produce spallation products via fragmentation of ^{16}O nuclei and capture of the generated neutrons [48]. The decay of these numerous products can mimic low-energy neutrino events and is a serious background. Super-Kamiokande has demonstrated [48, 49] that a cut on a likelihood function including spatial and temporal distance from the passing muon as well as energy loss of the muon can be used to efficiently remove spallation events. However this results in an additional 20% effective dead time for Super-Kamiokande while raising the threshold for neutrino detection to $\sim 15 \text{ MeV}$. As not all of the spallation and neutron capture cross-sections are known

and their calculation goes beyond the scope of this work, we cannot quantify this background. Yet, we note that Super-Kamiokande is located at a depth of 2700 meters water equivalent [50], comparable to the deep location considered here, and the passing muons should be equally well reconstructed, indicating that performance factors may be similar. A possible demonstration that this background can be controlled is left for future studies.

4.3. Solar neutrino background

Put aside the cosmic neutrino background—which is too low in energy to be detectable—the by far dominant flux of neutrinos at Earth comes from the Sun, where neutrinos are abundantly produced in several different fusion cycles [2]. As only ν_e and no $\bar{\nu}_e$ are generated in the Sun, solar neutrinos cannot undergo inverse beta-decay (IBD). The dominant interaction for solar neutrinos is elastic scattering on electrons (ES). Charged current interactions on oxygen nuclei are about two orders of magnitude less important [51] and are ignored here. Furthermore, only ${}^8\text{B}$ neutrinos need to be considered, since all other solar neutrino fluxes are too low in energy to be detectable in our configuration or well below the ${}^8\text{B}$ flux in magnitude [52, 53].

To calculate the interaction rate, we use an analytical expression for neutrino-electron elastic scattering (ES) from Eqn. (5.25) in [2]

$$\frac{d\sigma}{dT_e}(E_\nu, T_e) = \frac{\sigma_0}{m_e} \left[g_1^2 + g_2^2 \left(1 - \frac{T_e}{E_\nu}\right)^2 - g_1 g_2 \frac{m_e T_e}{E_\nu^2} \right] \quad (10)$$

with the kinetic energy of the recoil electron in the laboratory frame, T_e , and

$$\begin{aligned} \sigma_0 &= \frac{2 G_F^2 m_e^2}{\pi} \simeq 88.06 \cdot 10^{-46} \text{ cm}^2 \\ g_1 &= \begin{cases} \frac{1}{2} + \sin^2 \theta_W \simeq 0.73 & \text{for } \nu_e \\ -\frac{1}{2} + \sin^2 \theta_W \simeq -0.27 & \text{for } \nu_{\mu,\tau} \end{cases} \\ g_2 &= \sin^2 \theta_W \simeq 0.23 \end{aligned}$$

and fold it with the energy-dependent effective mass of our detector given in Fig. 7(b). Taking the shape of the ${}^8\text{B}$ neutrino spectrum from [54] and normalizing it to a total flux of $\Phi({}^8\text{B}) = 5 \cdot 10^6 \text{ cm}^{-2}\text{s}^{-1}$ [55] with components $\Phi_{\nu_e}({}^8\text{B}) = 1.7 \cdot 10^6 \text{ cm}^{-2}\text{s}^{-1}$ and $\Phi_{\nu_{\mu,\tau}}({}^8\text{B}) = 3.3 \cdot 10^6 \text{ cm}^{-2}\text{s}^{-1}$ [56], we arrive at an approximate solar neutrino event rate of 65 mHz. Additional application of local coincidence cleaning (cf. Sec.4.1.1) and the phase space cut (cf. Sec.4.1.2) reduces this rate to 30 mHz, still significantly larger than the maximum allowed rate of random background events $f_{\text{noise}}^{\text{BG}} = 1 \text{ mHz}$.

However, a number of methods can be applied to further diminish the rate of solar neutrino events. The bulk of solar neutrinos is less energetic than the bulk of SN neutrinos (cf. Fig. 7(a)). Changing the trigger requirement from 5 hits to 7 hits increases the energy threshold and

events per 10 s	solar ν_e	atm. $\nu_e + \bar{\nu}_e$	LL $\bar{\nu}_e$
5 hits, no cleaning	0.65	0.004	3.74
5 hits, RT+PS	0.30	0.003	2.76
6 hits, RT+PS	0.18	0.003	2.34
7 hits, RT+PS	0.10	0.003	1.91

Table 4: Average number of events per 10s from solar and atmospheric neutrino background (up to 100 MeV) as well as the SN neutrino signal for a LL supernova in 10 Mpc distance for different numbers of hit modules and with and without noise cleaning (RT+PS) applied.

thus reduces the expected event rate of solar neutrinos by a factor of three, while reducing the signal efficiency for SN neutrinos from the LL model by only 30%.

Alternatively, the electron emerging from the ES roughly keeps the direction of the incident neutrino, while the IBD effectively randomizes the positron direction. For a sufficiently densely instrumented array such as Super-Kamiokande, an angular resolution of about $\pm 30^\circ$ at $E_e = 10 \text{ MeV}$ is feasible [49, 51]. Assuming a one-sigma (68% of the events) angular cone of this size to reject neutrinos from the direction of the Sun, we cut away a solid angle of $\Omega_{\text{cut}} = 2\pi(1 - \cos 30^\circ)$ of the sky. We use this (instead of a cut on number of hits) to discriminate the solar neutrino rate to $f_\odot = (1 - 0.68)^3 \cdot 30 \text{ mHz} \approx 1 \text{ mHz}$, while retaining $(1 - \Omega_{\text{cut}}/(4\pi))^3 \approx 81\%$ of the SN events. While more efficient than a cut on the number of hits, the most powerful rejection will be achieved using a likelihood method that incorporates both the direction and energy for each event within the time window. In absence of a full reconstruction we refrain from a more detailed discussion, but note it as a requirement to reduce the large rate of solar neutrinos.

4.4. Atmospheric neutrino background

Cosmic rays colliding with the Earth’s atmosphere produce ν_e and $\bar{\nu}_e$ in similar abundance. The dominant component are the electron anti-neutrinos, interacting via IBD with a cross-section two orders of magnitude higher than the ES of electron neutrinos [49]. Taking the atmospheric neutrino flux calculations from [57], the ES cross-section from Eqn. 10 and the cross-section for IBD given in the phenomenological parametrization in [36] (“Naïve +” model), and integrating the event rate from 3 – 100 MeV, we arrive at an expected trigger level event rate of 0.004 mHz for ν_e and 0.4 mHz for $\bar{\nu}_e$ triggering on 5 hit sensors. The resulting spectrum, also shown in Figure 7 (d), peaks well above the peak of SN interactions, allowing to further discriminate these events. While somewhat more abundant, ES of ν_μ on e^- is only possible via neutral current interactions, and thus has a factor six smaller cross-section.

Another component of the background are *invisible muons* that are produced in the interactions of low-energy

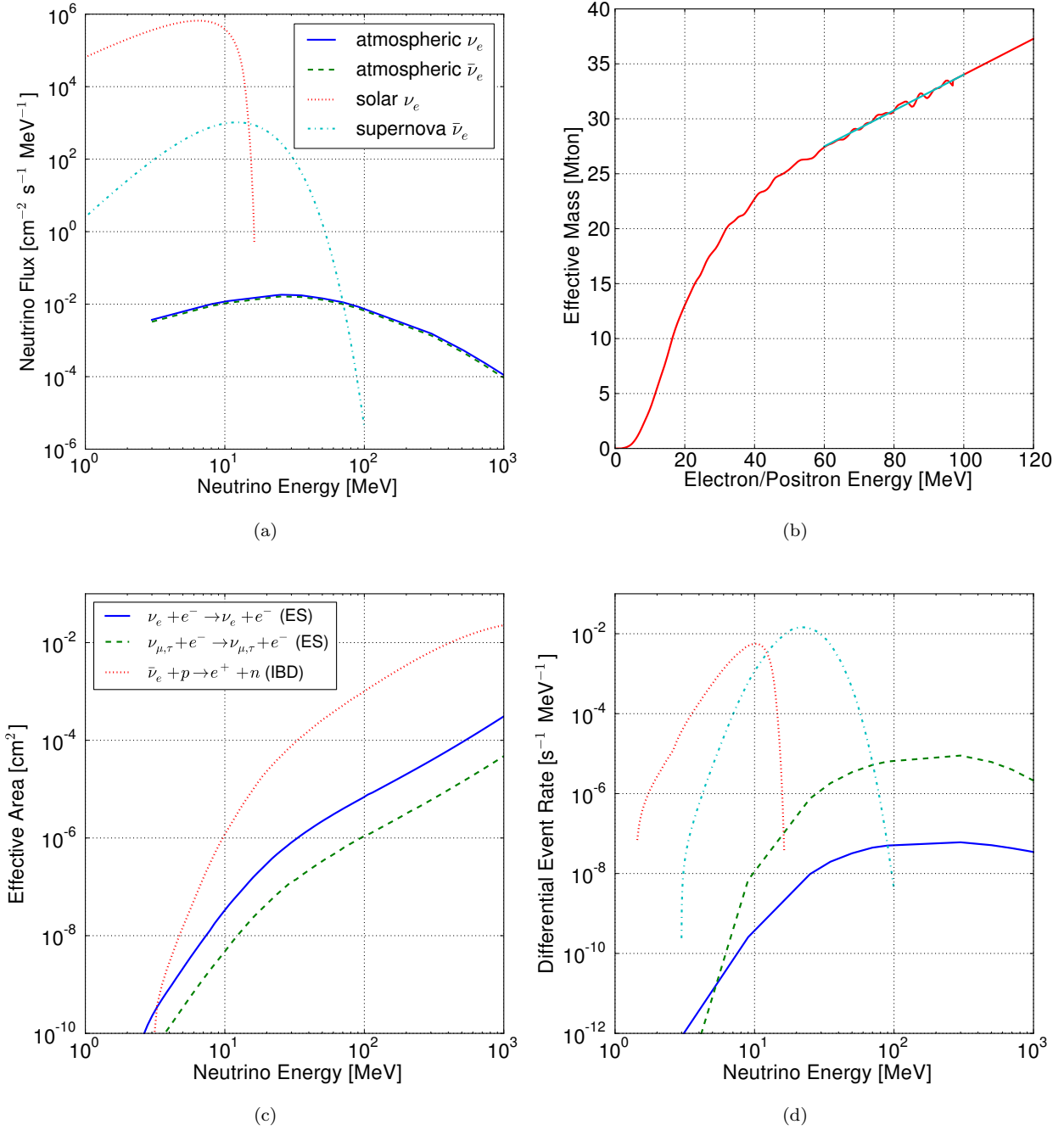


Figure 7: (a) The flux for solar [51, 54] and atmospheric [57] neutrinos as function of energy. The Supernova neutrino flux on Earth according to the LL model [30], normalized to an average power of $4.9 \cdot 10^{51} \text{ erg s}^{-1}$ in $\bar{\nu}_e$ for a supernova distance of 10 Mpc is shown assuming a burst duration of 10 s. (b) Effective mass as function of e^\pm energy, triggering on 5 hit modules, after applying noise cleaning down to $f_{\text{noise}}^{\text{cut}} = 1 \text{ mHz}$ for 10 Hz module noise. Above 100 MeV, a linear extrapolation (dashed) is used. (c) The effective area of the same detector for elastic scattering (ES) and inverse beta-decay (IBD), not including cuts to reject solar neutrinos. (d) Event rate per MeV as function of neutrino energy for solar, atmospheric and supernova neutrino fluxes from (a) with effective area from (c).

atmospheric muon neutrinos. The muons themselves are below the threshold for Cherenkov light emission and thus invisible. They can only travel few tens of centimeters and then decay to electrons which—due to their lower mass—can have a velocity above the Cherenkov threshold and become visible. These *Michel electrons* have been measured by Super-Kamiokande [49, 58] and amount to ~ 90 events per year in their effective volume of 22.5 ktons. At the peak energy of the Michel electron spectrum, 40 MeV, the effective mass of the detector simulated in this work is about 1000 times larger (see Fig. 7(b), so we can expect about 90000 events per year, or a rate of ≈ 3 mHz. While already small compared to the background of solar neutrinos, further reduction can be achieved by using the surrounding IceCube detector to veto accompanying atmospheric muons. Note that only invisible muons from muon neutrinos and not the atmospheric muons themselves can penetrate the detector and produce Michel electrons as, once below the Cherenkov threshold, the muons will decay within ~ 1 m.

4.5. Summary

The large sensor multiplicity requires intelligent trigger and selection algorithms to cope with the backgrounds arising from sensor self-noise, atmospheric muons, solar as well as atmospheric neutrinos. Despite making use of the event topology, the suppression of self-noise to a sufficiently low level will be a major challenge and requires future improvements in sensor development. Vetoing of atmospheric neutrinos and muons will result in some downtime in the detector. In particular, the discrimination of spallation products from muons passing the ice may pose a significant challenge and still has to be demonstrated. The dominant source of *physical* (i.e. neutrino) background stems from solar ${}^8\text{B}$ neutrinos, that need to be suppressed by reconstructing their direction and/or increasing the energy threshold.

5. Alternative detector location

An interesting alternative location for a Cherenkov detector in the South Pole ice is at a depth of 750 – 1050 m. It is known from measurements that at this depth the absorption length is exceptionally large with up to $\lambda_a \approx 350$ m [59]. However, the presence of air bubbles results in a very short scattering length of only $\lambda_e \approx 0.3$ m [59]. This results in an effective propagation length of $\lambda_p = \sqrt{\frac{\lambda_e \cdot \lambda_a}{3}} \sim 6$ m after which the photon flux has dropped by a factor e^{-1} [60]. The photons cannot travel large distances and are hence confined to a small volume for a rather long time of $\lambda_a/c \approx 1 \mu\text{s}$ before finally being absorbed. This leads to a large detection probability, given the light is emitted in the vicinity of a photo-sensor. The achievable effective mass at trigger level is thus several times larger than in the deep ice.

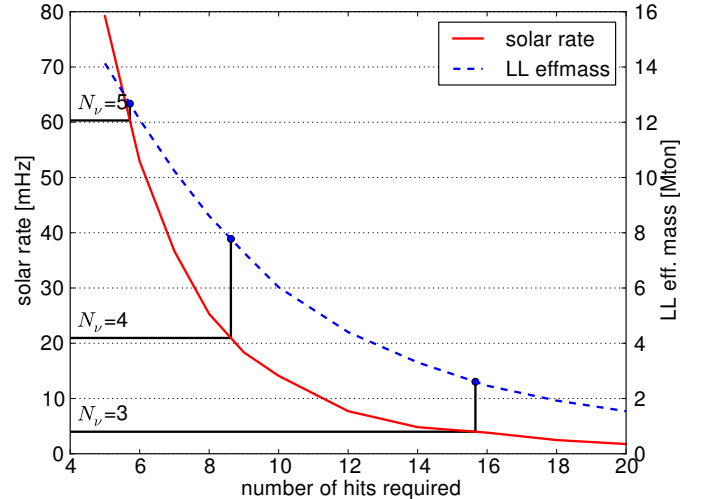


Figure 8: The solar neutrino event rate in the shallow ice detector (from neutrino-electron elastic scattering), together with the effective mass for SN neutrino events (Lawrence-Livermore), as a function of the number of hit modules required to trigger an event (which is a proxy of event energy). Horizontal lines indicate tolerable noise rates for a 1 second time window during which at least N_ν events shall make up a SN detection. The vertical lines point to the corresponding resulting effective mass.

We have simulated such a detector (same detector layout as in the deep ice) with an analytic description of the photon propagation (a random walk) using perfectly efficient cylindrical modules with 1 cm circumference and 1 m length, having an effective area comparable to HQE IceCube DOMs, roughly a factor 5.4 smaller than what was used in the deep ice. After applying the same optimized module noise cuts to reduce the self-noise rate to 1 mHz, one still obtains ~ 14 Mton effective mass, when triggering on 5 hit modules (including the higher dead time induced by atmospheric muons, conservatively estimated to 14% as explained in 4.2).

The main drawback of the shallow, diffusive ice is the lack of directional reconstruction of events. Due to the strong scattering, any information on the direction of the charged particle is lost. Among other things, this makes it impossible to veto elastic scattering events from solar neutrinos by their direction. Thus, a cut on the number of detected photons—which is directly proportional to the event energy and can be used as an energy proxy—is the only option to suppress that background. But due to the large overlap of the energy spectra of solar neutrinos and SN neutrinos (see Figure 7) one significantly loses detection efficiency.

Figure 8 shows the solar neutrino event rate and the effective mass for SN neutrinos (LL spectrum) as function of the number of hit modules required for the event trigger. Horizontal lines show the levels of solar event rate that can at most be tolerated, with the SN search window reduced

from 10 seconds to 1 second (thus missing about 40% of the SN neutrino events, according to Figure 1). For a number of neutrino events $N_\nu \geq 3$ per SN detection, a solar rate of ≈ 4 mHz can be allowed (see Eqn. 3). One would have to select events with at least 16 hit modules and the effective mass drops to about 2.5 Mtons. Increasing the number of instrumented modules or the modules' photo-effective area will not suffice to recover the effective mass, because the solar event rate would be increased as well.

Raising the neutrino event threshold N_ν relaxes the requirement on the solar rate—i.e. the cut on the hit modules—yielding a higher effective mass, but at the same time reducing the number of detected SNe. Optimizing again over all parameters, we find the best results for the shallow ice at $N_\nu = 5$ with a cut on at least 6 hit modules (c.f. Figure 8) in a SN search window of $\Delta t = 1$ s at an effective mass of about 12 Mton. However, only 60% of the SN neutrino events arrive within $\Delta t = 1$ s, (c.f. Figure 1), adding a factor $0.6^5 \approx 8\%$ to the supernova detection rate. In contrast, in the deep ice we are already at the optimum for a minimal N_ν of 3, with a SN search window of $\Delta t = 10$ s with a collection efficiency of nearly 100%, yielding an effective mass of 13.1 Mton. The achieved SN detection rates are compared in Table 6, revealing that the shallow ice is inferior to the deep ice.

Other physics cases such as proton decay also rely on directional information and cannot be pursued in the shallow ice. Additionally, the detector in the shallow ice will suffer more from other backgrounds as well, above all the atmospheric muons (much longer dead time) and muon-induced spallation events that might even become unmanageable in the low depth. Also, IceCube cannot be used as a veto in the shallow ice. Therefore, we disfavor a detector located in the shallow, diffusive ice.

6. Expected supernova detection rate

Knowing the detector effective area as a function of neutrino energy (Figure 7(c)), we can proceed to calculate the sensitivity to a supernova neutrino burst with a given spectrum. The probability to detect a supernova is calculated from Poisson statistics. We consider a supernova as detected if at least three neutrino events trigger the detector within 10 s, which is the threshold we can expect if all other backgrounds can be controlled to within 1 mHz. Figure 9 shows the SN detection probability as function of distance to the SN using the three considered models, with cuts applied against 10 Hz dark noise of the modules and against solar neutrinos (see Section 4). The distance up to which ≥ 3 neutrinos will be detected with a probability of $\geq 50\%$ is found to be 6.6 Mpc for the TBP model, 9.3 Mpc for the LL model and 25.5 Mpc for the dark SN model, respectively.

With this probability at hand along with the supernova rate in the local environment, we can compute the rate of expected supernova detections. We start from a catalog

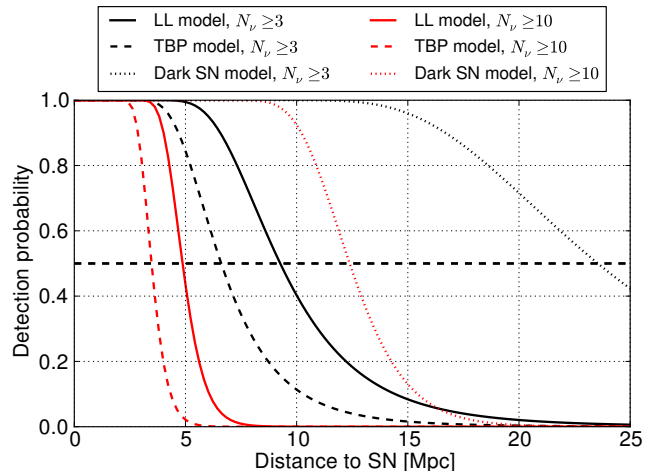


Figure 9: SN detection probability for the simulated detector after application of cuts as described in Section 4. Shown are results for the LL model, the TBP model, and a dark supernova model (compare Table 1) for the detection of at least either 3 or 10 neutrino events from the SN.

Galaxy	Type	SN Rate [SNu]
Elliptical	E-S0	< 0.05
Spiral-like	S0a-Sb	0.89 ± 0.33
Spiral	Sbc-Sd	1.68 ± 0.60
Others	Sm, Irr., Pec.	1.46 ± 0.71

Table 5: The expected rates of core-collapse supernovae for different galaxy types in supernova units ($1 \text{ SNu} = 1 \text{ SN}(100 \text{ yr})^{-1}(10^{10} L_{\odot}^{\text{B}})^{-1}$). Values from [62], scaled by 1.68 (see text).

of nearby galaxies that goes up to 100 Mpc [61]. Following [62] we assume that the blue luminosity of a galaxy is proportional to the star formation rate and hence also to the supernova rate. The conversion factor will depend on the galaxy type and is obtained from SN observations (cf. Table 5). These conversion factors lead to a total SN rate that is lower by a factor 1.68 compared to a more recent result derived from a comprehensive compilation of local SNe [63]. We include this additional scale factor in our rate estimate to ensure consistency with currently available data. For a limited number of galaxies, the catalog leaves the type unspecified. Testing the allowed range of conversion factors, this leads to an error $\leq 4\%$ on the total core-collapse SN rate for distances up to 20 Mpc.

Comparing with a theoretical prediction based on the initial mass function and cosmological star formation rate [9], our SN rate is still a factor two lower. One explanation might be that the conversion factors in Table 5 are based on observations with a bias to miss many faint SNe. Another possibility is a significant contribution of dark supernovae, that would not be detected optically, but still

	N_ν	CCSNe (LL)		CCSNe (TBP)	Dark SNe
		deep	shallow	deep	deep
L_\odot^B	≥ 3	20.4	3.1	10.3	17.4
	≥ 4	13.0	6.0	7.0	11.9
	≥ 5	9.9	7.4	5.4	8.4
	≥ 6	8.2	7.0	4.4	6.3
	≥ 7	7.0	6.0	3.7	4.8
	≥ 10	4.9	-	2.3	2.7
SFR	≥ 3	40.9	6.1	20.6	34.8
	≥ 10	9.8	-	4.5	5.4

Table 6: Expected number of supernova detections within one decade based on SN rates computed from the blue luminosity L_\odot^B of galaxies [62, 63] (first 6 lines). The last two lines are for a prediction scaled to match the star formation rate (SFR) [9] (c.f. Figure 10). Dark SNe are assumed to occur at a fraction of 10% of all core-collapse SNe (CCSNe). For the LL model, values for the simulated shallow ice detector (see Section 5) are listed as well.

emit neutrinos [9]. Scaling our blue luminosity prediction by a factor of two, we also find good agreement with the observed rate of nearby SNe [64], and regard the rate estimates based on actual observations of SNe and those scaled to the star formation rate—both shown in Figure 10—as lower and upper limit, respectively.

Table 6 gives a summary of expected SN detections per decade in different neutrino event multiplicity bins. The total resulting number of SN detections with the cuts described in Section 4 ranges from 20 to 41 per decade for the LL model and about half of that for the TBP model. For dark SNe, we make the assumption that SNe collapse to a black hole at a rate of 10% of the regular core-collapse SN rate. Yet due to a more energetic neutrino spectrum, dark SNe are detected at a higher efficiency resulting in between 17 and 35 dark observations per decade, comparable to the number of detections from the LL model. Altogether, one can expect to observe at least one SN per year on average, perhaps up to 5 or more. The rate of SNe producing strong bursts of ten or more neutrinos is between 0.2 and 0.5 per year without dark SNe, reaching up to almost 1 event per year if dark SNe are included. Note that while for a neutrino multiplicity of three, the event is as likely to be from a SN as from detector noise or solar background, a single event with a multiplicity of four (five) already constitutes a SN signal of $\sim 2\sigma$ ($\sim 4\sigma$). Yet, the true power of the approach lies in the combination with follow-up missions, that can detect the same SN in the optical or X-ray regime.

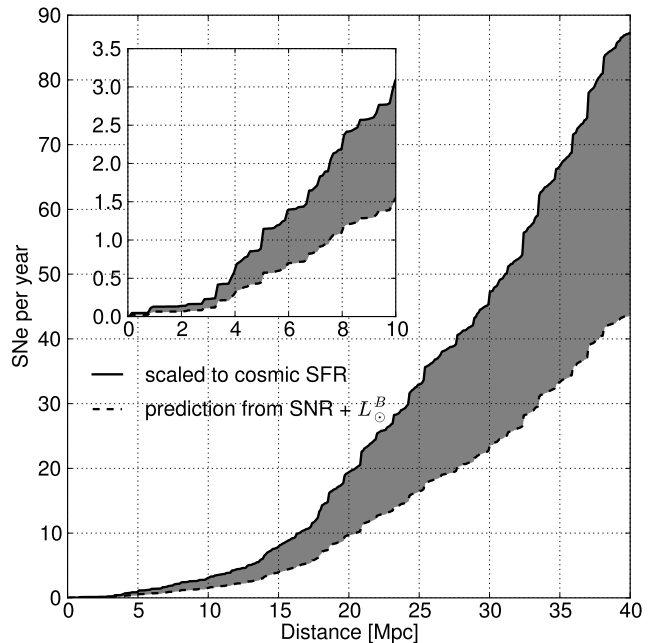


Figure 10: Range of cumulative expected supernova rate: lower curve (dashed) according to observed SN rate and blue luminosity [62], normalized to the results of [63], upper curve (solid) scaled by a factor 2 to match expectations from the cosmic star formation rate [9]. The galaxy distribution and their blue luminosity values are taken from [61].

7. Conclusion

A $\mathcal{O}(10)$ Mton scale neutrino detector is required to extend the sensitivity to core-collapse SNe beyond the Large Magellanic Cloud to neighboring galaxies and yield a detection rate of up to several SNe per year. In this paper, we have explored an implementation of such a detector in the very clear Antarctic ice at around 2300 m depth below surface where photons can travel with very little scattering. The detector geometry would resemble that of IceCube, however, with a much reduced string spacing and significantly increased density of photo-sensors per meter. Such a detector could be built in a similar manner as IceCube, by drilling holes into the ice and deploying strings holding the light sensors. To achieve the $\mathcal{O}(10)$ Mton detector with sensitivity to 10 MeV neutrinos at trigger level would require a 127-string installation with about 50 times the total photocathode area used in IceCube, indicating the demand for new and cheaper technology and dedicated R&D for photo-sensors with large effective photo-cathode area. Work in this direction has already been initiated and is embedded into the IceCube low-energy extension project PINGU (see [22], section 14). Efforts include the use of wavelength-shifters [45] and of multiple small PMTs within a single module similar to the KM3NeT optical modules [65]. Besides the large effective area, we identify a low noise rate as crucial requirement for the sensors.

Above a self-noise rate of ~ 50 Hz per meter instrumented string, it becomes difficult to retain the $\mathcal{O}(10)$ megaton target effective mass when exploitation the spatial and temporal distribution of hits to suppress sensor self-noise.

The main physical background remaining after the self-noise reduction arises due to solar ^8B neutrinos. These can be identified via lower photon multiplicity or—contingent on the ability to reconstruct their direction—by their angular proximity to the Sun. Atmospheric muons will provide exceedingly bright events in such a dense installation, resulting in a small downtime for the deep ice. More challenging is the rejection of Michel electron events, yet with the IceCube detector fully surrounding the array, their identification will be straight-forward and only a modest performance reduction will arise from their rejection. Muon induced spallation events need to be suppressed using temporal and spatial correlations with the originating muon and require more detailed studies including accurate description of the nuclear processes as well as full event reconstruction, which are both beyond the scope of this paper.

Using a catalog of nearby galaxies, we have computed the rate of detectable SN neutrino bursts. We show that depending on the SN rate and explosion model assumed, we can expect to observe between 10 and 41 SNe per decade in neutrinos (not counting the dark SNe). By combining the observation of a neutrino burst with an optical detection of a SN, one can thereby disentangle the question of explosion model and SN rate. We note that in the future, with large, wide field optical surveys covering essentially the full sky, nearby SNe should be found in an even more systematic manner than today [66, 67].

Dark supernovae, where the star collapses to a black hole, could produce more than 20 detectable bursts per decade. Such a SN can be indirectly identified through the absence of an optical counterpart (with the risk of confusing it with a regular, dust obscured SN), or more directly, by observing neutrinos of higher energies. The limited energy resolution of the detector ($\approx 30\%$ per neutrino event) should be sufficient to estimate the effective temperature of the neutrino emission and hence the origin of the burst.

A neutrino detector as described in this paper will not only yield a precise measurement of the local supernova rate and can uncover dark supernovae. A few of the supernovae will be closer, or perhaps even galactic, and hence yield a much higher number of coincident neutrinos, allowing to infer details about the explosion or even the neutrino mass hierarchy [68, 69]. To conclude, we point out that the low energy threshold and very large effective mass make such a detector potentially interesting for a number of other physics phenomena, including e.g. proton decay studies and solar neutrino analysis. While we have demonstrated that one can achieve the desired goal—routine observation of SNe in neutrinos—we acknowledge the assumptions we have made on our way. In particular, we have identified the development of large-area low-noise photo-sensors, suitable for deployment in the ice at South

Pole, as a key requirement.

Acknowledgements

We would like to thank Imre Bartos, John Beacom, Francis Halzen, Allan Hallgren, and Lutz Köpke for fruitful discussions, as well as the IceCube collaboration for graciously allowing us to use its photon tracking software. We acknowledge support from the Helmholtz Alliance for Astroparticle Physics (HAP).

References

- [1] W. Arnett, Supernova 1987A (1989). doi:10.1146/annurev.astro.27.1.629.
- [2] C. Giunti, C. Kim, Fundamentals of neutrino physics and astrophysics, Oxford University Press, 2007.
- [3] G. Raffelt, Supernova neutrino observations: What can we learn?, arXiv:astro-ph/0701677v2.
- [4] A. S. Dighe, Physics potential of future supernova neutrino observations, arXiv:0809.2977v3.
- [5] M. Ikeda, A. Takeda, Y. Fukuda, et al., Search for Supernova Neutrino Bursts at Super-Kamiokande, *Astrophys. J.* 669 (1) (2007) 519.
- [6] R. Abbasi, Y. Abdou, T. Abu-Zayyad, et al., IceCube sensitivity for low-energy neutrinos from nearby supernovae, *Astronomy & Astrophysics* 535 (2011) A109. doi:10.1051/0004-6361/201117810.
- [7] S. Ando, J. F. Beacom, H. Yüksel, Detection of Neutrinos from Supernovae in Nearby Galaxies, *Phys. Rev. Lett.* 95 (17) (2005) 171101. arXiv:astro-ph/0503321.
- [8] M. D. Kistler, H. Yüksel, S. Ando, et al., Core-Collapse Astrophysics with a Five-Megaton Neutrino Detector, *Phys. Rev. D* 83 (2011) 123008. arXiv:0810.1959.
- [9] S. Horiuchi, J. F. Beacom, C. S. Kochanek, et al., The Cosmic Core-collapse Supernova Rate does not match the Massive-Star Formation Rate, *Astrophys. J.* 738 (2011) 154–169. arXiv:1102.1977.
- [10] L. Yang, C. Lunardini, Revealing local failed supernovae with neutrino telescopes, *Phys. Rev. D* 84 (2011) 063002. arXiv:1103.4628.
- [11] Y. Sekiguchi, K. Kiuchi, K. Kyutoku, et al., Gravitational waves and neutrino emission from the merger of binary neutron stars, arXiv:1105.2125.
- [12] B. Dasgupta, T. Fischer, S. Horiuchi, M. Liebendorfer, A. Mirizzi, et al., Detecting the QCD phase transition in the next Galactic supernova neutrino burst, *Phys. Rev. D* 81 (2010) 103005. arXiv:0912.2568.
- [13] R. M. Humphreys, K. Davidson, The luminous blue variables: Astrophysical geysers, *Publ. Astron. Soc. Pac.* 106 (1994) 1025–1051. doi:10.1086/133478.
- [14] S. Ando, K. Sato, Relic neutrino background from cosmological supernovae, *New J. Phys.* 6 (1) (2004) 170.
- [15] G. Pagliaroli, F. Rossi-Torres, F. Vissani, Neutrino mass bound in the standard scenario for supernova electronic antineutrino emission, *Astroparticle Physics* 33 (5–6) (2010) 287–291.
- [16] K. Nakamura, Hyper-Kamiokande: A next generation water Cherenkov detector, *Int. J. Mod. Phys. A* 18 (2003) 4053–4063.
- [17] K. Abe, T. Abe, H. Aihara, et al., Letter of Intent: The Hyper-Kamiokande Experiment — Detector Design and Physics Potential, arXiv:1109.3262.
- [18] C. K. Jung, Feasibility of a next generation underground water Cherenkov detector: UNO, *AIP Conf. Proc.* 533 (2000) 29–34. arXiv:hep-ex/0005046.
- [19] A. Creusot, The Antares detector, *Nucl.Instrum.Meth.* A718 (2013) 489–491. doi:10.1016/j.nima.2012.11.071.
- [20] T. DeYoung, Neutrino Astronomy with IceCube, *Mod. Phys. Lett. A* 24 (2009) 1543–1557. arXiv:astro-ph/0906.4530.

- [21] L. Demirors, M. Ribordy, M. Salathe, Novel technique for supernova detection with IceCube, [arXiv:1106.1937v2](#).
- [22] M. Aartsen, et al., Letter of Intent: The Precision IceCube Next Generation Upgrade (PINGU), [arXiv:1401.2046](#).
- [23] E. K. Akhmedov, S. Razzaque, A. Y. Smirnov, Mass hierarchy, 2-3 mixing and CP-phase with Huge Atmospheric Neutrino Detectors, [arXiv:1205.7071](#).
- [24] R. Abbasi, et al., The Energy Spectrum of Atmospheric Neutrinos between 2 and 200 TeV with the AMANDA-II Detector, *Astropart.Phys.* 34 (2010) 48–58. [arXiv:1004.2357](#), doi:10.1016/j.astropartphys.2010.05.001.
- [25] A. Achterberg, et al., First Year Performance of The IceCube Neutrino Telescope, *Astropart.Phys.* 26 (2006) 155–173. [arXiv:astro-ph/0604450](#), doi:10.1016/j.astropartphys.2006.06.007.
- [26] R. Abbasi, et al., The Design and Performance of IceCube DeepCore, *Astropart.Phys.* 35 (2012) 615–624. [arXiv:1109.6096](#), doi:10.1016/j.astropartphys.2012.01.004.
- [27] M. Aartsen, et al., Evidence for High-Energy Extraterrestrial Neutrinos at the IceCube Detector, *Science* 342 (6161) (2013) 1242856. [arXiv:1311.5238](#), doi:10.1126/science.1242856.
- [28] I. Bartos, A. Beloborodov, K. Hurley, S. Marka, Detection Prospects for GeV Neutrinos from Collisionally Heated Gamma-ray Bursts with IceCube/DeepCore, [arXiv:1301.4232](#).
- [29] K. Murase, K. Kashiyama, P. Meszaros, Subphotospheric Neutrinos from Gamma-Ray Bursts: The Role of Neutrons, [arXiv:1301.4236](#).
- [30] T. Totani, K. Sato, H. E. Dalhed, et al., Future Detection of Supernova Neutrino Burst and Explosion Mechanism, *Astrophys. J.* 496 (1) (1998) 216.
- [31] N. Schmitz, *Neutrino Physik*, 1st Edition, Teubner Studienbücher: Physik, Teubner, 1997.
- [32] T. A. Thompson, A. Burrows, P. A. Pinto, Shock Breakout in Core-Collapse Supernovae and its Neutrino Signature, *Astrophys. J.* 592 (2003) 434.
- [33] H. T. Janka, Explosion Mechanisms of Core-Collapse Supernovae, [arXiv:1206.2503](#).
- [34] K. Nakazato, K. Sumiyoshi, H. Suzuki, et al., Oscillation and Future Detection of Failed Supernova Neutrinos from Black Hole Forming Collapse, *Phys. Rev. D* 78 (2008) 083014. [arXiv:0810.3734](#).
- [35] K. Sumiyoshi, S. Yamada, H. Suzuki, S. Chiba, Neutrino signals from the formation of black hole: A probe of equation of state of dense matter, *Phys. Rev. Lett.* 97 (2006) 091101. [arXiv:astro-ph/0608509](#).
- [36] A. Strumia, F. Vissani, Precise quasielastic neutrino nucleon cross section, *Phys. Lett. B* 564 (2003) 42–54. [arXiv:astro-ph/0302055](#).
- [37] M. Ackermann, et al., Optical properties of deep glacial ice at the South Pole, *J. Geophys. Res.* 111 (D13) (2006) D13203+.
- [38] M. Aartsen, others (IceCube collaboration), Measurement of South Pole ice transparency with the IceCube LED calibration system, *Nucl.Instrum.Meth.* A711 (0) (2013) 73 – 89.
- [39] J. Lundberg, P. Miocinovic, K. Woschnagg, et al., Light tracking through ice and water – Scattering and absorption in heterogeneous media with Photonics, *Nucl.Instrum.Meth.* A581 (3) (2007) 619 – 631. [arXiv:astro-ph/0702108](#).
- [40] K. Woschnagg, Photonics Web Page.
URL <http://icecube.berkeley.edu/kurt/photonics/>
- [41] A. Olivás, D. Chirkin, K. Hoshina, et al., Photonics at sourceforge.net.
URL <http://photonics.sourceforge.net>
- [42] R. Abbasi, et al., The IceCube Data Acquisition System: Signal Capture, Digitization, and Timestamping, *Nucl.Instrum.Meth.* A601 (2009) 294–316. [arXiv:0810.4930](#).
- [43] R. Abbasi, et al., Calibration and Characterization of the IceCube Photomultiplier Tube, *Nucl.Instrum.Meth.* A618 (2010) 139–152. [arXiv:1002.2442](#).
- [44] S. Böser, M. Kowalski, L. Köpke, L. Schulte, M. Voge, A Single Photon Sensor employing Wavelength-shifting and Light-guiding Technology, in preparation.
- [45] L. Schulte, M. Voge, A. Hoffmann, S. Böser, L. Köpke, et al., A large-area single photon sensor employing wavelength-shifting and light-guiding technology, [arXiv:1307.6713](#).
- [46] J. Ahrens, J. Bahcall, X. Bai, et al., Sensitivity of the IceCube detector to astrophysical sources of high energy muon neutrinos, *Astroparticle Physics* 20 (5) (2004) 507 – 532.
- [47] E. V. Bugaev, et al., Atmospheric muon flux at sea level, underground and underwater, *Phys. Rev. D* 58 (1998) 054001. [arXiv:hep-ph/9803488](#).
- [48] K. Bays, et al., Supernova Relic Neutrino Search at Super-Kamiokande, *Phys. Rev. D* 85 (2012) 052007. [arXiv:1111.5031](#), doi:10.1103/PhysRevD.85.052007.
- [49] M. Malek, M. Morii, S. Fukuda, et al., Search for Supernova Relic Neutrinos at Super-Kamiokande, *Phys. Rev. Lett.* 90 (2003) 061101.
- [50] Y. Fukuda, et al., Measurements of the solar neutrino flux from Super-Kamiokande’s first 300 days, *Phys. Rev. Lett.* 81 (1998) 1158–1162. [arXiv:hep-ex/9805021](#).
- [51] W. Haxton, R. Robertson, Solar neutrino interactions with O-18 in Super-Kamiokande, *Phys. Rev. C* 59 (1999) 515–519. [arXiv:nucl-th/9806081](#).
- [52] J. N. Bahcall, C. Pena-Garay, Solar models and solar neutrino oscillations, *New J. Phys.* 6 (2004) 63. [arXiv:hep-ph/0404061](#).
- [53] J. N. Bahcall, A. M. Serenelli, S. Basu, New solar opacities, abundances, helioseismology, and neutrino fluxes, *Astrophys. J.* 621 (2005) L85–L88. [arXiv:astro-ph/0412440](#).
- [54] J. N. Bahcall, E. Lisi, D. E. Alburger, et al., Standard neutrino spectrum from ^8B decay, *Phys. Rev. C* 54 (1996) 411–422.
- [55] B. Aharmim, et al., Low Energy Threshold Analysis of the Phase I and Phase II Data Sets of the Sudbury Neutrino Observatory, *Phys. Rev. C* 81 (2010) 055504. [arXiv:0910.2984](#), doi:10.1103/PhysRevC.81.055504.
- [56] B. Aharmim, et al., Electron energy spectra, fluxes, and day-night asymmetries of B-8 solar neutrinos from measurements with NaCl dissolved in the heavy-water detector at the Sudbury Neutrino Observatory, *Phys. Rev. C* 72 (2005) 055502. [arXiv:nucl-ex/0502021](#), doi:10.1103/PhysRevC.72.055502.
- [57] T. Gaisser, T. Stanev, G. Barr, Cosmic Ray Neutrinos in the Atmosphere, *Phys. Rev. D* 38 (1988) 85.
- [58] J. F. Beacom, The Diffuse Supernova Neutrino Background, *Ann.Rev.Nucl.Part.Sci.* 60 (2010) 439–462. [arXiv:1004.3311](#).
- [59] R. A. Porrata, The Energy Spectrum of Pointlike Events in AMANDA-A, PhD dissertation, University of California (1997).
- [60] P. Askebjerg, S. W. Barwick, L. Bergström, et al., Optical properties of deep ice at the South Pole: absorption, *Appl. Opt.* 36 (18) (1997) 4168–4180.
- [61] D. J. White, E. J. Daw, V. S. Dhillon, A List of Galaxies for Gravitational Wave Searches, *Class.Quant.Grav.* 28 (8) (2011) 085016. [arXiv:1103.0695](#).
- [62] E. Cappellaro, R. Evans, M. Turatto, A new determination of supernova rates and a comparison with indicators for galactic star formation, *Astronomy & Astrophysics* 351 (1999) 459. [arXiv:astro-ph/9904225](#).
- [63] W. Li, R. Chornock, J. Leaman, et al., Nearby supernova rates from the Lick Observatory Supernova Search - III. The rate-size relation, and the rates as a function of galaxy Hubble type and colour, *Mon. Not. R. Astron. Soc.* 412 (2010) 1473–1507. [arXiv:1006.4613](#).
- [64] S. Horiuchi, J. F. Beacom, M. S. Bothwell, T. A. Thompson, Effects of stellar rotation on star formation rates and comparison to core-collapse supernova rates, [arXiv:1302.0287](#).
- [65] O. Kavatsyuk, Q. Dorosti-Hasankiadeh, H. Löhner, Multi-PMT optical module for the KM3NeT neutrino telescope, *Nucl.Instrum.Meth.* 695 (0) (2012) 338 – 341. doi:10.1016/j.nima.2011.09.062.
- [66] Z. Ivezić, J. Tyson, R. Allsman, J. Andrew, R. Angel, LSST: from Science Drivers to Reference Design and Anticipated Data Products, [arXiv:0805.2366](#).
- [67] S. Kulkarni, Cosmic Explosions (Optical Transients), [arXiv:1202.2381](#).
- [68] A. S. Dighe, M. T. Keil, G. G. Raffelt, Detecting the neutrino

mass hierarchy with a supernova at IceCube, JCAP 0306 (2003) 005. [arXiv:hep-ph/0303210](#).

- [69] P. D. Serpico, S. Chakraborty, T. Fischer, L. Hudepohl, H.-T. Janka, et al., Probing the neutrino mass hierarchy with the rise time of a supernova burst, Phys.Rev. D85 (2012) 085031. [arXiv:1111.4483](#).